

# Triple-Band Polarization Angle Independent $90^\circ$ Polarization Rotator Based on Fermat's Spiral Structure Planar Chiral Metamaterial

Yongzhi Cheng<sup>1, 2, \*</sup>, Wangyang Li<sup>1, 2</sup>, and Xuesong Mao<sup>1, 2</sup>

**Abstract**—We propose a planar chiral metamaterial (PCMM), which can function as a triple-band polarization angle independent  $90^\circ$  polarization rotator. The unit cell of the PCMM is composed of bi-layered mutual twisted Fermat's spiral structure (FSS) resonators with four-fold rotation symmetry. The simulated and measured results show that the PCMM can work in triple-band and convert a linearly polarized ( $y$ -/ $x$ -polarized) wave to its cross-polarization ( $x$ -/ $y$ -polarized) or experience a near  $90^\circ$  polarization rotation with a polarization conversion ratio of over 90%. The electric field and surface current distributions of the unit-cell structure are analyzed to study its physics mechanism. Compared with previous CMM-based rotator, our design has more operation frequencies in a single PCMM structure, a relative thinner thickness, and higher  $Q$ -factor. Good performances of the PCMM suggest promising applications in the polarization rotator or convertor that need to be integrated with other compact devices.

## 1. INTRODUCTION

Polarization as one of the most important and basic characteristics of electromagnetic (EM) waves or lights plays a vital role in many optoelectronic systems or classical physical effects since it carries the information about chirality, spin orientation, and microscopic anisotropy [1–4]. Controlling and manipulating the polarization states of EM waves show great promise for a variety of applications including optoelectronics analytical chemistry, and biological sciences, which have been explored extensively from microwave to optical regions [5–10]. Polarization rotator or convertor is an efficient polarization manipulation device that can rotate the polarization plane of an incident linearly polarized EM wave by a fixed angle, while maintaining its linearly polarized nature in transmission or reflection mode. Hence, polarization rotator or convertor is highly desirable for polarization manipulation. Conventional methods to manipulate polarization state of EM waves usually make use of polarization analyzers and wave plates based on the liquid crystals, anisotropic media or Faraday Effect [11, 12]. However, in those approaches there usually exist some inherent drawbacks, such as narrow band response, large material thickness, and integration difficulty in current optoelectronic systems. Over the past few years, metamaterials (MMs) as artificial composite materials or structures composed of sub-wavelength periodic unit-cells have achieved some exotic EM properties unavailable in nature, such as anomalous refraction/reflection [9] and polarization conversion [10]. Particularly, two kinds of MMs have been proposed and demonstrated polarization conversion [5–10]. The first one is anisotropic MMs, similar to the birefringent crystals, which is sensitive to the polarization azimuth angle of the incident

---

*Received 26 November 2018, Accepted 29 April 2019, Scheduled 29 July 2019*

\* Corresponding author: Yongzhi Cheng (cyz0715@126.com).

<sup>1</sup> Engineering Research Center for Metallurgical Automation and Detecting Technology Ministry of Education, Wuhan University of Science and Technology, 430081, China. <sup>2</sup> School of Information Science and Engineering, Wuhan University of Science and Technology, Wuhan, Hubei 430081, China.

wave [5, 6, 10]. The other is chiral metamaterial (CMM), which has experientially demonstrated that it can provide extremely strong polarization rotatory power due to its extrinsic chirality [13–15]. Generally, the giant polarization rotation realized with CMM is several orders of magnitude larger than that of conventional natural materials. Compared with conventional devices or methods [16, 17], CMM has several advantages, such as flexible manipulation range of the operation wavelength and high efficiency, revealing that it is very suitable for polarization manipulation [13–31].

Significant efforts have been devoted to the realization of various CMMs in converting or rotating the polarization of EM wave with high efficiency [22–31]. Essentially, these special CMMs structures for polarization rotations or conversions with high efficiency mainly originate from their extrinsic chirality induced by the EM coupling effects. These CMMs structures have been proposed to obtain cross polarization waves in transmission, which can exhibit cross polarization conversion or giant optical activity by 90° linear polarization rotation [32–36]. These CMMs structures are usually constructed by bi-layered or triple-layered enantiomeric metallic patterns sandwiched with dielectric substrates [18–34]. However, these CMM structures are not transversely isotropic, usually working with a very low cross-polarization transmission, single frequency band or polarization angle dependent response. These drawbacks have taken some adverseness on its application in optics devices. To overcome these deficiencies, some novel CMM structures have been proposed and demonstrated. For example, a bi-layered CMM is proposed by Ye and He, which can realize a giant optical activity by 90° polarization rotation originated from the transverse magnetic dipole coupling among metallic wire pairs [13]. Then, a composite CMM based on triple-layered metallic structures was proposed by Mutlu and Ozbay, which can achieve 90° polarization rotation with high efficiency by combining EM wave tunneling and chirality [34]. Recently, a CMM based on twisted electric field coupled resonators was proposed by Shi et al., which can realize a dual-band 90° polarization rotation with polarization angle insensitive in microwave region [35]. Then, a new CMM based on a spiral slot structure was proposed by Tang et al., and dual-band cross-polarization conversion could be realized in terahertz region [36]. However, the transmission coefficient of cross-polarization is relatively small, and current designs of CMMs are mainly concentrated on dual bands, which could hamper their practical engineering applications. Thus, it is very important to design a new type of CMMs for 90° polarization rotation or cross polarization conversion operated at multi-band with polarization angle independent response.

In this work, a novel planar CMM (PCMM) based on a Fermat’s spiral structure (FSS) is proposed and studied numerically and experimentally, which can achieve cross-polarization conversion with polarization angle independent or 90° polarization rotation. The simulation results exhibit that the incident linear polarization will be converted to its orthogonal direction or experience 90° polarization rotation at 4.20 GHz, 7.45 GHz, and 10.88 GHz, respectively, which is independent of the polarization azimuth angle, and agree well with experiment. The physical origin of the cross polarization conversion is illustrated by analyzing the surface current and electric field distributions of the unit-cell structure of the proposed PCMM. Compared with previous reported CMMs for polarization rotators [31–36], our design has some advantages: Firstly, our PCMM has an ultra-thin thickness and novel resonance mechanism. Secondly, the simple design of the PCMM has more operation frequencies in a single patterned metallic structure and is also polarization-insensitive for normal incident waves. Thirdly, our design has a relatively high  $Q$  factor. Such an effective design of PCMM may provide some potential applications in antenna, sensing, detection, or telecommunication systems.

## 2. FUNDAMENTAL THEORY ANALYSIS

Firstly, we briefly recall some fundamental theories of CMMs for polarization manipulation before characterizing the EM characteristics of our design. Under the Cartesian coordinates of  $x$ - $y$ - $z$ , considering an incident EM field  $\mathbf{E}^i$  propagating in the  $+z$  direction, the expressions of electric field vector of incident and transmitted wave along  $x$ -axis and  $y$ -axis direction can be written as [37]:

$$\mathbf{E}^i(r, t) = \begin{pmatrix} E_x^i \\ E_y^i \end{pmatrix} e^{i(kz - \omega t)} \quad (1a)$$

$$\mathbf{E}^t(r, t) = \begin{pmatrix} E_x^t \\ E_y^t \end{pmatrix} e^{i(kz - \omega t)} \quad (1b)$$

where  $\omega, k, E_x$ , and  $E_y$  represent the angular frequency, wave vector, and complex amplitudes of electric fields, respectively. The transmission coefficient is defined as  $t_{ij} = E_j^t/E_j^i$  in terms of the ratio of the electric fields, with the first and second subscripts  $i$  and  $j$  ( $= x, y$  for linear polarization,  $= +, -$  for circular polarization) denoting the polarization states of the transmitted and incident wave components, respectively. It indicates that an arbitrary linear polarization wave through a chiral system can be decomposed into components of the transmitted EM waves  $E_x^t$  and  $E_y^t$  through the above transmission coefficients (the complex Jones matrix,  $T_{li}$ ). Considering an incident linear polarization wave propagating along the  $-z$  direction, the Jones matrix  $T_{li}$  formulations for linear polarization wave can be expressed as [7]:

$$\begin{pmatrix} T_x \\ T_y \end{pmatrix} = T_{li} \begin{pmatrix} E_x^i \\ E_y^i \end{pmatrix} = \begin{pmatrix} t_{xx} & t_{xy} \\ t_{yx} & t_{yy} \end{pmatrix} \begin{pmatrix} E_x^i \\ E_y^i \end{pmatrix} \quad (2)$$

To characterize the linear polarization rotation or conversion efficiency of the transmitted waves for incident different ( $x$ -polarization and  $y$ -polarization) linear polarization waves, we usually define the polarization conversion ratio (PCR) as:

$$\text{PCR}_x = |t_{yx}|^2 / (|t_{yx}|^2 + |t_{xx}|^2) \quad (3a)$$

$$\text{PCR}_y = |t_{xy}|^2 / (|t_{xy}|^2 + |t_{yy}|^2) \quad (3b)$$

where  $\text{PCR}_x$  and  $\text{PCR}_y$  correspond to the normal incident  $x$ - and  $y$ -polarization waves, respectively. Without absorption and diffractions, when the cross-polarization transmission coefficients are near unity ( $t_{xy} \approx 1, t_{yx} \approx 1$ ) and the co-polarization transmission coefficients near zero ( $t_{xx} \approx 0, t_{yy} \approx 0$ ), we can get  $\text{PCR}_x = 1$  and  $\text{PCR}_y = 1$ , respectively. The magnitude of PCR close to 100% means that an incident linear polarization wave can be converted to its cross-polarization component completely after transmission. Thus, the conversion efficiency should be as high as possible for the linear polarization convertor or 90° polarization rotator.

Under the circular polarization base, considering an incident linear polarization wave propagating along the  $-z$  direction, the conversion relation of the transmission coefficients of linear and circular polarization waves can be given as:

$$T_{cir} = \begin{pmatrix} t_{++} & t_{+-} \\ t_{-+} & t_{--} \end{pmatrix} = \frac{1}{2} \times \begin{pmatrix} (t_{xx} + t_{yy}) + i(t_{xy} - t_{yx})(t_{xx} - t_{yy}) - i(t_{xy} + t_{yx}) \\ (t_{xx} - t_{yy}) + i(t_{xy} + t_{yx})(t_{xx} + t_{yy}) - i(t_{xy} - t_{yx}) \end{pmatrix} \quad (4)$$

where  $t_{++}, t_{--}, t_{+-}$ , and  $t_{-+}$  are the circular polarization transmission coefficients and obtained to fully characterize the response of the CMMs. For the  $C_4$  rotational symmetry of the proposed CMMs, the two cross-polarization transmission coefficients and two co-polarization transmission coefficients are approximately assumed as  $t_{xx} = t_{yy}$  and  $t_{xy} = -t_{yx}$ , respectively. The cross circular polarization transmissions  $t_{+-}$  and  $t_{-+}$  are near zero due to the fourfold rotational symmetry of the proposed CMMs. Thus, the relational expression between the circular polarization wave ( $T_+$  and  $T_-$ ) and linear polarized wave ( $T_x$  and  $T_y$ ) can be given as follows:

$$t_{++/-} = t_{yy} \pm it_{xy} = t_{xx} \mp it_{yx} \quad (5)$$

Optical activity and circular dichroism are the two important properties of CMMs, which can be characterized by the polarization azimuth rotation angle ( $\theta$ ) and ellipticity ( $\eta$ ), respectively.  $\theta$  means the changing rotation angle between the polarization planes ( $E$ -plane) of the out wave and incident wave.  $\eta$  denotes the difference of polarization state of out wave and incident wave.  $\theta$  and  $\eta$  can be expressed by the following formulas:

$$\theta = \frac{1}{2} [\arg(t_{++}) - \arg(t_{--})] \quad (6)$$

$$\eta = \arctan \left( \frac{|t_{++}| - |t_{--}|}{|t_{++}| + |t_{--}|} \right) \quad (7)$$

where  $t_{++}$  and  $t_{--}$  are referred to the field amplitude of left circular polarization (LCP,  $-$ ) and right circular polarization (RCP,  $+$ ) waves. If  $\eta = \pm 45^\circ$  and  $0^\circ$ , the out wave will be purely circular and linear polarization, respectively; otherwise, if  $|\eta| < 45^\circ$ , the out wave will be elliptical polarization.

### 3. UNIT-CELL STRUCTURE DESIGN, SIMULATION AND EXPERIMENT

Generally, it is difficult to realize a linear polarization rotation up to  $90^\circ$  with a high efficiency of cross-polarization conversion in previous CMM based on the mutual twisted resonator structures [7, 14, 15, 22–28]. Another CMM based on some longitudinal magnetic dipole coupling has been proposed to get strong rotatory strength [13, 34–36]. To achieve multi-band  $90^\circ$  polarization rotation with a polarization angle independent response, a special PCMM structure with fourfold-rotational ( $C_4$ ) symmetry is desirable to excite the multiple resonance mode for normal incident linear polarization wave. For the previous CMM structures, only electric or magnetic resonance mode can be excited, thus resulting in a single or dual-band polarization rotation property. The FSS and its complementary structure has been proposed and demonstrated that it could produce the magnetic and electric localized surface plasmons (LSPs) resonance for normal incident linear polarization wave due to its longer spiral structure [38, 39]. Recently, bi-layered FSS was designed for the CMM, which possesses both electric and magnetic dipole coupling responses for linear to circular polarization conversion [25]. The bi-layered conjugated FSS is chosen for the PCMM design since it is relatively compact compared with a normal Archimedean spiral structure [25]. Therefore, based on the bi-layered FSS, it also inspires us to construct PCMM with cross-polarization conversion or giant optical activity by  $90^\circ$  polarization rotation. Figs. 1(a) and (b) present the unit-cell structure design schematics of the proposed PCMM, which consists of bi-layer conjugated FSSs separated by a dielectric substrate. The bi-layered mutually twisted quad-filar system is built by placing four FSS arms with  $90^\circ$  rotational arrangements. Thus, it can form a fourfold-rotational ( $C_4$ ) symmetric PCMM, which will be independent from the polarization angle of the incident wave. As shown in Fig. 1(a) (see the red dashed line), each spiral has a spiral turn of 2, and the spiraling constant of  $r = a\sqrt{2\pi}/\sqrt{\text{rad}} \text{ mm}$  is used to design the unit-cell structure of the PCMM, where  $a$  is the spiral parameter representing the degree of spiraling for the given number of turns. Similar to previous reported designs [25, 38, 39], the average diameter of the spiral of the FSS is two times less than the

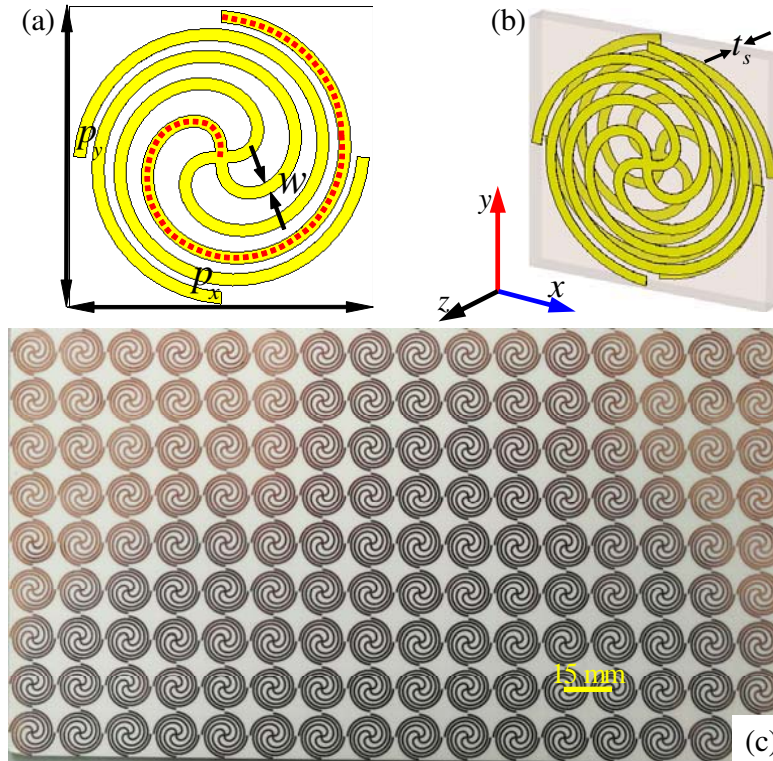


**Figure 1.** (a), (b) The front view and perspective view of the unit-cell structure of the designed PCMM, (c) a portion of photograph of the fabricated sample.

normal spiral, which can significantly reduce the transverse dimension of the unit-cell structure. It can be expected that the designed PCMM structure based on FSS can excite different resonance modes for the normal incident linear polarization wave, thus resulting in a multi-band polarization rotation. In the  $x$ - $y$  plane, the geometry parameter of each FSS wire should obey the equation:  $x = r \cdot \cos(r^2/a^2)$ ,  $y = r \cdot \sin(r^2/a^2)$ . The optimized geometry parameters are as follow:  $p_x = p_y = 15$  mm,  $t_s = 1.5$  mm,  $w = 0.6$  mm,  $a = 2.8$  mm. A low loss dielectric substrate Rogers R04003 is chosen as the middle spacer layer, and the relative dielectric constant and loss tangent are 3.55 and 0.0027. The bi-layered conjugated quad-filar FSS layers in both sides of the dielectric substrate are modeled as a 0.035 mm copper film with a frequency-independent conductivity of  $\sigma = 5.8 \times 10^7$  S/m.

To study EM properties of the designed PCMM, the numerical simulations as well as experiments were performed. The numerical calculation simulations were carried out via the three-dimensional high frequency EM simulation software CST Microwave Studio, using the frequency solver based on the finite integration technology (FIT). In simulation, the unit cell boundary conditions were used in  $x$  and  $y$  directions ( $x$ - $y$  plane) to replicate an infinite planar array, and the open boundary conditions were used in the  $z$  direction. In addition, the transmission can be expressed by means of complex Jones matrices, where transmission coefficient  $t_{ij} = E_j^t/E_i^i$  is defined in terms of the complex amplitude of the electric field of the transmitted and incident waves. The first and second subscripts  $i$  and  $j$  ( $= x, y$  for linear polarization,  $= +, -$  for circular polarization) represent the polarization states of the transmitted/incident wave components, respectively.

In practical experiment, we fabricated the PCMM test sample by the traditional printed circuit board (PCB) process according to the above optimized geometric parameters, and a portion of the sample photograph is given in Fig. 1(c). The total dimension of the fabricated PCMM sample is 240 mm  $\times$  240 mm  $\times$  1.57 mm, containing 16  $\times$  16 unit cells. The sample was measured through free-space EM wave transmission measurement in a microwave anechoic chamber. In an EM anechoic chamber, two double-ridged broadband horn antennas connected to a vector network analyzer (Agilent PNA-X N5244A) were used to measure transmission properties of the fabricated sample. In practical measurement, the PCMM slab sample was placed in the middle position of the horn antennas. To eliminate the near-field effect, the two antennas own VSWR  $< 2$  were distributed by a distance of 2 m in a wide frequency range of 3–13 GHz [40]. When performing measurement, the time-domain gating strategy was used to eliminate the undesirable repetitively reflected EM waves. When a broadband plane EM wave with  $y(x)$ -polarization ( $E$  field in the  $y(x)$ -axis direction) normally passed through the PCMM slab along  $-z$  direction, the transmission coefficients of  $t_{yy}$ ,  $t_{xx}$ ,  $t_{xy}$ , and  $t_{yx}$  can be obtained, where the first and second subscripts denote the polarization of the transmitted and incident waves, respectively.

#### 4. RESULTS AND DISCUSSIONS

Firstly, we numerically and experimentally investigate the transmission coefficients of the linearly polarized wave through the PCMM as shown in Fig. 2. In Fig. 2, we present the measured and simulated linear polarization transmission matrix elements ( $t_{xx}$ ,  $t_{yy}$ ,  $t_{xy}$ , and  $t_{yx}$ ) of the proposed PCMM for the forward ( $-z$  direction) propagating waves, respectively. The simulated results are in agreement qualitatively with the experimental ones, except for a slight red shift. The possible reasons for these undesired deviations can include: 1) the difference of the EM parameters (e.g., permittivity) of the dielectric substrate, 2) the small differences in substrate and metal thicknesses due to the fabrication imperfection, and 3) the tiny distortion and finite size effects in measurement should also be considered.

As shown in Figs. 2(a), (b), three resonance frequencies for simulation (measurement) can be observed evidently,  $f_1 = 4.19$  (4.21) GHz,  $f_2 = 7.45$  (7.62) GHz, and  $f_3 = 10.88$  (10.96) GHz. The corresponding electric thickness of the PCMM is about  $\lambda_1/45.38$ ,  $\lambda_2/25.07$  and  $\lambda_3/17.43$ , respectively, where  $\lambda_i$  ( $i = 1, 2, 3$ ) is corresponding to the resonance wavelength. Thus, our designed PCMM slab possesses an ultrathin thickness compared with the operation wavelength ( $< \lambda/17.43$ , at 10.96 GHz). Owing to the  $C_4$  rotational symmetry of the unit-cell structure of the PCMM, it is obvious that two co-polarization transmission coefficients are equivalent and that two cross-polarization transmission coefficients are equivalent ( $t_{xx} = t_{yy}$  and  $t_{yx} = t_{xy}$ ), respectively. From Fig. 2(a), at resonance frequencies of 4.19 (4.21) GHz, 7.45 (7.62) GHz, and 10.88 (10.96) GHz, the co-polarization transmissions

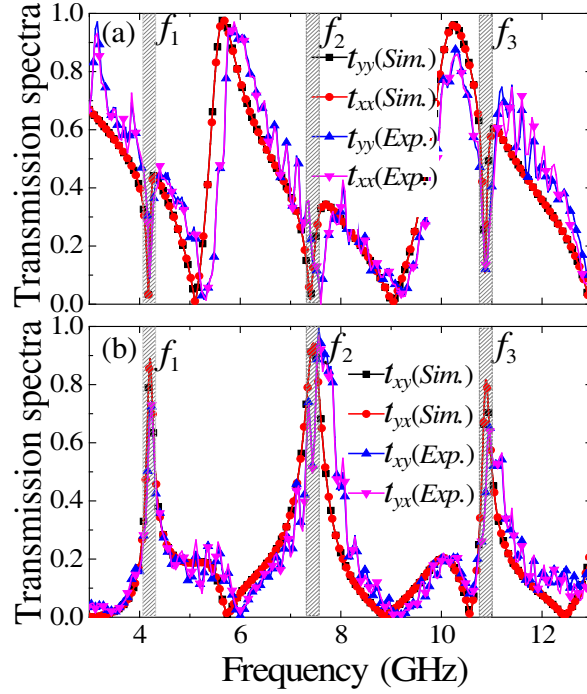


**Figure 2.** The simulated and measured (a) co-polarization ( $t_{xx}$  and  $t_{yy}$ ) and (b) cross-polarization ( $t_{xy}$  and  $t_{yx}$ ) transmission coefficients for the normal incident EM wave propagation along  $-z$  direction.

$t_{xx}$  and  $t_{yy}$  are both decreased to the minimal values about 0.03(0.095), 0.017(0.0014), and 0.11(0.13), respectively. From Fig. 2(b), at above same resonance frequencies, the cross-polarization transmissions  $t_{yx}$  and  $t_{xy}$  are both increased to the maximal values about 0.88(0.73), 0.93(0.96), and 0.81(0.65), respectively. In addition, the cross-polarization transmission line shapes at resonance frequencies are very sharp. The full widths at half maximum (FWHM) of cross-polarization transmission at three step resonance frequencies are about 0.18 GHz, 0.53 GHz, and 0.2 GHz, respectively. We then calculated the  $Q$ -factor, defined as the ratio of the central frequency to FWHM bandwidth of cross-polarization transmission. The corresponding values of  $Q$ -factor are about 23.3, 14.1, and 54.4, respectively. Thus, it can be expected that the proposed PCMM has some potential applications in sensing or detection due to its higher  $Q$ -factor. These results suggest that the incident  $y(x)$ -polarized wave propagation through the PCMM slab will be converted into its cross-polarization components or experience a near  $90^\circ$  polarization rotation in transmission at above three resonance frequencies.

To verify the efficiency of the designed PCMM, the polarization conversion ratio (PCR) was usually used to characterize the linear polarization conversion or rotation efficiency of the out waves, which are expressed in Eqs. (3a) and (3b). The PCR and cross-polarization transmission should be as high as possible in engineering. Thus, the high efficiency for  $x$ -to- $y$  ( $y$ -to- $x$ ) polarization conversion or near  $90^\circ$  polarization rotation can be unambiguously demonstrated. Figs. 3(a) and (b) present simulated and measured  $\text{PCR}_y$  and  $\text{PCR}_x$  for normal incident  $y$ -polarized and  $x$ -polarized wave, respectively. It can be seen that the simulated (measured)  $\text{PCR}_y$  is about 99.8 (98.4)%, 99.8 (99.9)%, and 98.1 (93.8)% at 4.19 (4.21) GHz, 7.45 (7.62) GHz, and 10.88 (10.96) GHz, respectively, for normal incident  $y$ -polarization waves (see Fig. 3(a)). For normal incident  $x$ -polarization waves, as shown in Fig. 3(b), the simulated (measured)  $\text{PCR}_x$  is about 99.8 (98.1)%, 99.9 (99.9)%, and 98.1 (93.3)% at above resonance frequencies, respectively. We also find that the simulated  $\text{PCR}_{x(y)}$  is greater than 90% at 5.1 GHz and 9 GHz, respectively. However, in those frequencies for  $\text{PCR}_{x(y)} > 90\%$ , the cross-polarization transmission coefficients are below 0.3, implying that there is very small EM wave through the PCMM slab. These results further demonstrate that an incident  $x(y)$ -polarization wave can be converted to its cross-polarization with a conversion efficiency of over 90% by the designed PCMM slab after transmission at resonances.

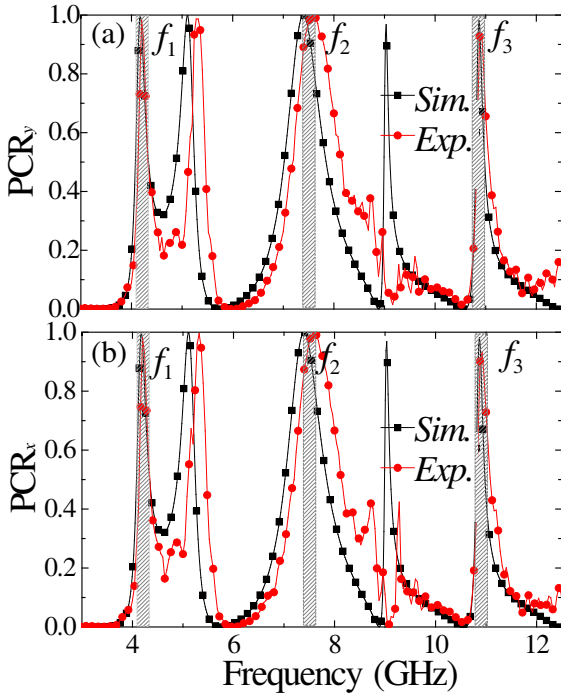


**Figure 3.** Simulated and measured polarization conversion ratio (PCR) for the incident (a)  $y$ -polarized and (b)  $x$ -polarized wave along  $-z$  direction.

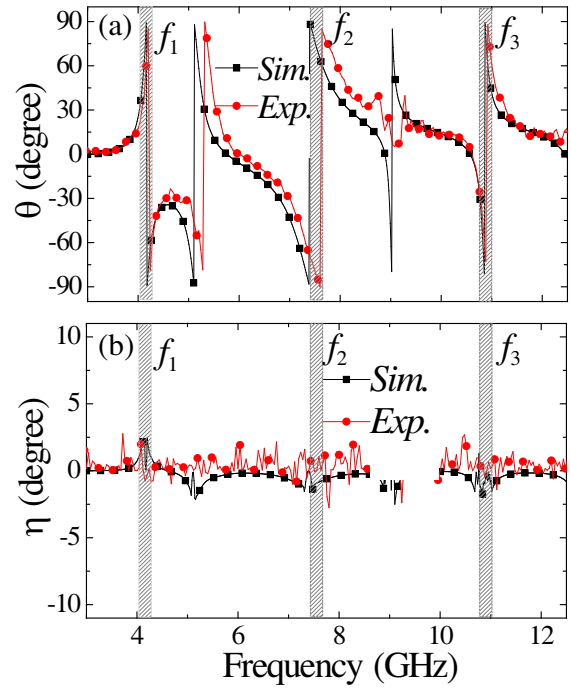


**Figure 4.** Simulated and measured (a) polarization azimuth rotation angle ( $\theta$ ) and (b) ellipticity ( $\eta$ ) for the forward ( $-z$ ) propagation.

To further illustrate the polarization rotation characteristic of transmitted EM waves, we calculated the polarization rotation angle ( $\theta$ ) and ellipticity ( $\eta$ ) angle according to Eqs. (6) and (7). Figs. 4(a) and (b) present the simulated and measured  $\theta$  and  $\eta$  for normal incident  $y$ -polarization wave propagation along forward ( $-z$ ) direction, respectively. We can see that the simulated (measured)  $\theta$  is about  $88.98^\circ$  ( $85.05^\circ$ ),  $99.98^\circ$  ( $84.53^\circ$ ), and  $89.19^\circ$  ( $93.8^\circ$ ) while the absolute value of the  $\eta$  is less than  $3^\circ$  at 4.19 (4.21) GHz, 7.45 (7.62) GHz, and 10.88 (10.96) GHz, respectively. It means that the out wave is still linear polarization with rotation angle about  $90^\circ$  at above three resonance frequencies and also indicating giant optical activity. These results confirm that the transmitted waves experience a near  $90^\circ$  polarization rotation with a near pure optical activity at above resonance frequencies, respectively.

To verify the linear polarization angle independent of our designed PCMM slab, we simulated and measured the cross-polarization transmission coefficient ( $t_{xy}$ ) when the sample was rotated up to  $45^\circ$  about  $z$  axis with a step of  $15^\circ$  with different polarization angles ( $\varphi$ ) of the incident electric field respect to the  $y$ -axis, as shown in Figs. 5(a) and (b). It can be observed that both simulated and measured  $t_{xy}$  are not obviously changed with the variation of  $\varphi$  at above three resonance frequencies due to  $C_4$  rotational symmetry of the unit-cell structure of the proposed PCMM. These results further confirm that a triple-band  $90^\circ$  polarization rotator using the proposed PCMM slab can operate efficiently for any polarization azimuth.

In order to illustrate the cross-polarization conversion mechanism of the proposed PCMM, we performed the surface current analysis by simulating the surface current distributions of the unit-cell structure at resonance frequencies, as shown in Figs. 6(a), (b), and (c). The previous research results indicate that the polarization conversion of the bi-layered conjugated FSSs mainly originates the electric and magnetic dipole coupling excited for normal incident linear polarization wave [25]. From Fig. 6(a), at the lower frequency of 4.19 GHz, it can be observed that the surface currents flow directions in the front and back layers of the unit-cell structure are the same and oscillate symmetrically, implying electric dipole coupling interactions. It is similar to the entire mirror symmetric structure that excites the electric dipole coupling for normal incident linear polarization wave [41, 42]. At the second frequency

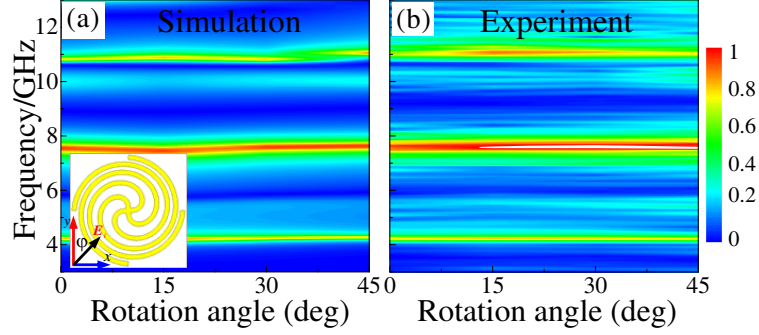


**Figure 5.** The (a) simulated and (b) measured cross-polarization transmission coefficient ( $t_{xy}$ ) of the proposed PCMM with different polarization angle ( $\varphi$ ) of the incident electric field respect to the  $y$ -axis.

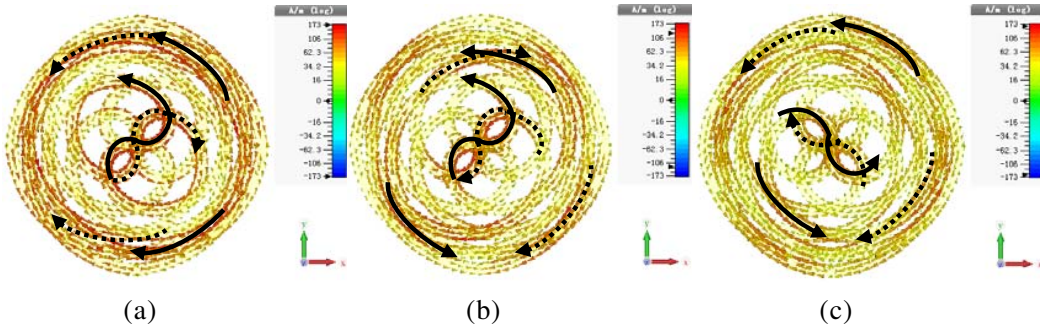


**Figure 6.** The simulated surface currents distributions of the unit-cell structure for the proposed PCMM in the case of incident  $y$ -polarized wave propagating along  $-z$  direction at (a)  $f_1 = 4.19$  GHz, (b)  $f_2 = 7.45$  GHz, (c)  $f_3 = 10.88$  GHz. The solid and dash line arrow indicate the surface current flow direction of the front and back layer structure.

of 7.45 GHz, as shown in Fig. 6(b), the surface currents flow directions in the front and back layers of the unit-cell structure are antiparallel and oscillating anti-symmetrically, revealing magnetic dipole coupling interactions. At the third frequency of 10.88 GHz, as shown in Fig. 6(c), the surface currents in the front and back layers of the unit-cell structure oscillate not only symmetrically but also anti-symmetrically, implying both electric and magnetic dipoles coupling interactions. So, the unit-cell structure of the PCMM resonates as electric and magnetic dipoles due to the symmetric and anti-symmetric current distributions at above three frequencies. These symmetric and anti-symmetric current distributions induce electric and magnetic dipoles coupling interactions which contribute to nearly  $90^\circ$  polarization rotation or cross-polarization transmission strongly at resonances. These results further indicate that triple-band perfect nearly  $90^\circ$  polarization rotation is mainly due to the combination of the electric and magnetic resonance responses. In addition, it can be expected that quad-band and multi-band  $90^\circ$  polarization rotation properties could also be realized by selecting appropriate geometric parameters of the proposed PCMM (e.g., selecting longer spiral structure).

To more intuitively elucidate the linear polarization rotation or conversion properties of the proposed PCMM, we analyzed the evolution of electric fields in the  $y$ - $z$  plane when the incident  $y$ -polarization waves are propagating along  $-z$  direction at resonance frequencies. From Figs. 7(a)–(c), it can be observed that the incident electric field ( $E_{in}$ ) along the  $+y$  axis direction will be converted to the transmitted electric field ( $E_{out}$ ) along the  $+x$  axis direction, revealing that the incident  $y$ -polarization wave is converted to the outgoing  $x$ -polarization wave or experiencing a  $90^\circ$  polarization rotation at resonance frequencies. It should be noticed that the incident  $x$ -polarization wave can also be converted to the outgoing  $y$ -polarization wave or experiencing a  $90^\circ$  polarization rotation at the same resonance frequencies (not shown). It means that the incident  $y(x)$ -polarization ( $E_{in}$  is along  $+y(+x)$  direction) waves propagating along backward ( $-z$ ) direction from the front metallic structure excites the guided

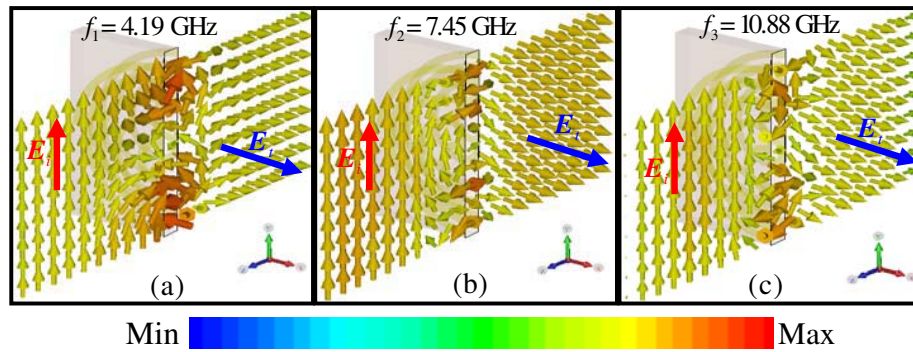


**Figure 7.** Simulated electric field distributions for the proposed PCMM in the case of the incident  $y$ -polarization wave along  $-z$  direction at different resonance frequencies: (a)  $f_1 = 4.19$  GHz, (b)  $f_2 = 7.45$  GHz, (c)  $f_3 = 10.88$  GHz. Bold arrows qualitatively indicate the direction strength of electric field.

resonant modes of the unit-cell structure and are finally near perfectly converted to the transmitted  $x(y)$ -polarization ( $E_{out}$  is along  $+x(+y)$  direction) wave. In addition, all incident field patterns will be twisted inside the bi-layered conjugated structure as a consequence of strong chirality of the proposed PCMM [14, 20, 27]. These electric field distributions pictures of the unit-cell structure are excellently consistent with results of the polarization azimuth rotation angle  $\theta$  and ellipticity  $\eta$ . Thus, these results further validate that the proposed PCMM slab can function as a triple-band cross-polarization convertor or homogeneous  $90^\circ$  polarization rotator.

## 5. CONCLUSION

In conclusion, we present a design, simulation, and experiment of an ultrathin triple-band polarization angle independent  $90^\circ$  polarization rotator based on PCMM in microwave region. The unit-cell structure of the PCMM consists of a dielectric sandwiched with bi-layered conjugated FSS. Both simulation and experiment results show that the  $90^\circ$  polarization rotator exhibits strong cross-polarization transmission with a high efficiency (the PCR is more than 95% on average) at resonance frequencies. The  $90^\circ$  polarization rotator based on the PCMM has a relatively thin thickness, which is about  $1/45.38$ ,  $1/25.07$ , and  $1/17.43$  of the operation wavelengths, respectively. In addition, the values of  $Q$ -factor are about 23.3, 14.1, and 54.4, respectively. Moreover, the proposed triple-band  $90^\circ$  polarization rotator can work efficiently for any polarization azimuth due to the  $C_4$  rotational symmetry. The analyses of the current distributions indicate that the cross-polarization or  $90^\circ$  polarization rotation is mainly due to the electric and magnetic coupling interactions. The triple-band  $90^\circ$  polarization rotator could be potential applied in some multi-band sensing, detection, communication, and antenna systems due to its high performances (thin thickness, high  $Q$ -factor, high polarization conversion efficiency, and polarization angle independent).

## ACKNOWLEDGMENT

This work was supported by the National Natural Science Foundation of China (Grant No. 61605147), the Science and Technology Research Project of Education Department of Hubei China (Grant No. D20181107), and the Natural Science Foundation of Hubei province (Grant No. 2017CFB588).

## REFERENCES

1. Saleh, B. E. A. and M. C. Teich, *Fundamentals of Photonics*, Wiley, New Jersey, 2007.
2. Zhao, Y., M. A. Belkin, and A. Alù, "Twisted optical metamaterials for planarized ultrathin broadband circular polarizers," *Nat. Commun.*, Vol. 3, 870, 2012.

3. Yao, B., M. Lei, L. Ren, N. Menke, Y. Wang, T. Fischer, and N. Hampp, "Polarization multiplexed write-once-read-many optical data storage in bacteriorhodopsin films," *Opt. Lett.*, Vol. 30, No. 22, 3060–3062, 2005.
4. Sherif, E., H. Mohamed, H. Mohamed, and E. A. Soliman, "E-shaped wideband plasmonic nanennas with linear and dual-linear polarizations," *Photon. Res.*, Vol. 3, 140145, 2015.
5. Hao, J., Y. Yuan, L. Ran, T. Jiang, J. A. Kong, C. T. Chan, and L. Zhou, "Manipulating electromagnetic wave polarizations by anisotropic metamaterials," *Phys. Rev. Lett.*, Vol. 99, 063908, 2007.
6. Chin, J. Y., M. Lu, and T. J. Cui, "Metamaterial polarizers by electric-field-coupled resonators," *Appl. Phys. Lett.*, Vol. 93, 251903, 2008.
7. Cheng, Y. Z., Y. Nie, X. Wang, and R. Z. Gong, "An ultrathin transparent metamaterial polarization transformer based on a twist-split-ring resonator," *Appl. Phys., A Mater. Sci. Process.*, Vol. 111, No. 1, 209215, 2013.
8. He, Q., S. L. Sun, S. Y. Xiao, X. Li, Z. Y. Song, W. J. Sun, and L. Zhou, "Manipulating electromagnetic waves with metamaterials: Concept and microwave realizations," *Chin. Phys. B*, Vol. 23, No. 4, 047808, 2014.
9. Huang, C., X. Ma, M. Pu, G. Yi, Y. Wang, and X. Luo, "Dual-band 90° polarization rotator using twisted split ring resonators array," *Opt. Commun.*, Vol. 291, 345–348, 2013.
10. Xiong, X., Y. Hu, S. Jiang, Y. Hu, R. Fan, G. Ma, D. Shu, R. Peng, and M. Wang, "Metallic stereostructured layer: An approach for broadband polarization state manipulation," *Appl. Phys. Lett.*, Vol. 105, 201105, 2014.
11. Chen, C. Y., T. R. Tsai, C. L. Pan, and R. P. Pan, "Effect of carbon nanotube doping on critical current density of MgB<sub>2</sub>/MgB<sub>2</sub> superconductor," *Appl. Phys. Lett.*, Vol. 83, 4497, 2003.
12. Masson, J. B. and G. Gallot, "Terahertz achromatic quarter-wave plate," *Opt. Lett.*, Vol. 31, No. 2, 265–267, 2006.
13. Ye, Y. and S. He, "90° polarization rotator using a bilayered chiral metamaterial with giant optical activity," *Appl. Phys. Lett.*, Vol. 96, 203501, 2010.
14. Cheng, Y., Y. Nie, Z. Cheng, and R. Z. Gong, "Dual-band circular polarizer and linear polarization transformer based on twisted split-ring structure asymmetric chiral metamaterial," *Progress In Electromagnetics Research*, Vol. 145, 263–272, 2014.
15. Huang, Y., Z. Yao, Q. Wang, F. Hu, and X. Xu, "Coupling Tai Chi chiral metamaterials with strong optical activity in terahertz region," *Plasmonics*, Vol. 10, No. 4, 1005–1011, 2015.
16. Chen, C. Y., T. R. Tsai, C. L. Pan, and R. P. Pan, "Room temperature terahertz phase shifter based on magnetically controlled birefringence in liquid crystals," *Appl. Phys. Lett.*, Vol. 83, 4497, 2003.
17. Yamada, I., K. Takano, M. Hangyo, M. Saito, and W. Watanabe, "Terahertz wire-grid polarizers with micrometer-pitch Al gratings," *Opt. Lett.*, Vol. 34, 274, 2009.
18. Wei, Z., Y. Cao, Y. Fan, X. Yu, and H. Li, "Broadband polarization transformation via enhanced asymmetric transmission through arrays of twisted complementary split-ring resonators," *Appl. Phys. Lett.*, Vol. 99, No. 22, 221907-3, 2011.
19. Xu, H.-X., G.-M. Wang, M.-Q. Qi, and T. Cai, "Dual-band circular polarizer and asymmetric spectrum filter using ultrathin compact chiral metamaterial," *Progress In Electromagnetics Research*, Vol. 143, 243–261, 2013.
20. Cheng, Y., Y. Nie, Z. Z. Cheng, L. Wu, X. Wang, and R. Z. Gong, "Broadband transparent metamaterial linear polarization transformer based on triple-split-ring resonators," *Journal of Electromagnetic Waves and Applications*, Vol. 27, No. 14, 1850–1858, 2013.
21. Ma, X., C. Huang, M. Pu, W. Pan, Y. Wang, and X. Luo, "Circular dichroism and optical rotation in twisted Y-shaped chiral metamaterial," *Appl. Phys. Exp.*, Vol. 6, 022001, 2013.
22. Grady, N. K., J. E. Heyes, D. R. Chowdhury, Y. Zeng, M. T. Reiten, A. K. Azad, A. J. Taylor, D. A. Dalvit, and H. T. Chen, "Terahertz metamaterials for linear polarization conversion and anomalous refraction," *Science*, Vol. 340, No. 6138, 1304–1307, 2013.

23. Song, K., Y. Liu, C. Luo, and X. Zhao, "High-efficiency broadband and multiband cross-polarization conversion using chiral metamaterial," *J. Phys. D: Appl. Phys.*, Vol. 47, 505104, 2014.
24. Han, S., H. Yang, L. Guo, X. Huang, and B. Xiao, "Manipulating linearly polarized electromagnetic waves using the asymmetric transmission effect of planar chiral metamaterials," *J. Opt.*, Vol. 16, No. 3, 035105, 2014.
25. Yogesh, N. F., T. Lan, and F. Ouyang, "Far-Infrared circular polarization and polarization filtering based on fermat's spiral chiral metamaterial," *IEEE Photonics Journal*, Vol. 7, No. 3, 1–12, 2015.
26. Gonulal, S., M. K., E. Unal, F. D. Kemal Delihacioglu, E. Tetik, and C. Sabah, "90° Polarization rotator and antireflector using meanderline chiral metamaterials: Analytical and numerical approach," *Optik*, Vol. 126, No. 24, 5587–5592, 2015.
27. Ma, X., Z. Xiao, and D. Liu, "Dual-band cross polarization converter in bi layered complementary chiral metamaterial," *Journal of Modern Optics*, Vol. 63, No. 10, 937–940, 2016.
28. Xu, K., Z. Xiao, J. Tang, D. Liu, and Z. Wang, "Ultra-broad band and dual-band highly efficient polarization conversion based on the three-layered chiral structure," *Physica E*, Vol. 81, 169–176, 2016.
29. Cheng, Y. Z., R. Z. Gong, and L. Wu, "Ultra-broadband linear polarization conversion via diode-like asymmetric transmission with composite metamaterial for terahertz waves," *Plasmonics*, Vol. 12, No. 4, 1113–1120, 2017.
30. Han, J., H. Li, Y. Fan, Z. Wei, C. Wu, Y. Cao, X. Yu, F. Li, and Z. Wang, "An ultrathin twist-structure polarization transformer based on fish-scale metallic wires," *Appl. Phys. Lett.*, Vol. 98, No. 15, 151908, 2011.
31. Huang C., Y. Feng, J. Zhao, Z. Wang, and T. Jiang, "Asymmetric electromagnetic wave transmission of linear polarization via polarization conversion through chiral metamaterial structures," *Phys. Rev. B*, Vol. 85, No. 19, 195131, 2012.
32. Song, K., X. Zhao, Y. Liu, Q. Fu, and C. Luo, "A frequency-tunable 90°-polarization rotation device using composite chiral metamaterials," *Appl. Phys. Lett.*, Vol. 103, 101908, 2013.
33. Shang, X., X. Zhai, L. Wang, M. He, Q. Li, X. Luo, and H. Duan, "Asymmetric transmission and polarization conversion of linearly polarized waves with bilayer L-shaped metasurfaces," *Appl. Phys. Express*, Vol. 10, 052602, 2017.
34. Mutlu, M. and E. Ozbay, "A transparent 90° polarization rotator by combining chirality and electromagnetic wave tunneling," *Appl. Phys. Lett.*, Vol. 100, 051909, 2012.
35. Shi, H., A. Zhang, S. Zheng, J. Li, and Y. Jiang, "Dual-band polarization angle independent 90° polarization rotator using twisted electric-field-coupled resonators," *Appl. Phys. Lett.*, Vol. 104, No. 3, 034102, 2014.
36. Tang, J., Z. Xiao, K. Xu, X. Ma, D. Liu, and Z. Wang, "Cross polarization conversion based on a new chiral spiral slot structure in THz region," *Opt. Quant. Electron.*, Vol. 48, 111, 2016.
37. Menzel, C., C. Rockstuhl, and F. Lederer, "Advanced Jones calculus for the classification of periodic metamaterials," *Physical Review A*, Vol. 82, No. 5, 053811, 2010.
38. Paloma A., X. S. Huidobro, J. Cuerda, E. Moreno, L. M. Moreno, and T. J. C. F. J Garcia-Vidal, and J. B. Pendry, "Magnetic localized surface plasmons," *Phys. Rev. X.*, Vol. 4, No. 2, 021003, 2014.
39. Gao, Z., F. Gao, Y. Zhang, and B. Zhang, "Complementary structure for designer localized surface plasmons," *Applied Physics Letters*, Vol. 107, 191103, 2015.
40. Cheng, Y., C. Wu, Z. Z. Cheng, and R. Z. Gong, "Ultra-compact multi-band chiral metamaterial circular polarizer based on triple twisted split-ring resonator," *Progress In Electromagnetics Research*, Vol. 155, 105–113, 2016.
41. Zhao, J. and Y. Z. Cheng, "Ultrathin dual-band polarization angle independent 90° polarization rotator with giant optical activity based on planar chiral metamaterial," *Applied Physics B*, Vol. 124, 185, 2018.
42. Cheng, Z. Z. and Y. Z. Cheng, "A multi-functional polarization convertor based on chiral metamaterial for terahertz waves," *Opt. Commun.*, Vol. 435, 178–182, 2019.